Pergamon

Chemical Engineering Science, Vol. 53, No. 20, pp. 3635–3652, 1998

Printed in Great Britain

PII: S0009–2509(98)00179–1

0009–2509/98/$–See front matter

Analysis of a Taylor–Poiseuille vortex flow reactor—I: Flow patterns and mass transfer characteristics

R. C. Giordano,*,† R. L. C. Giordano,* D. M. F. Prazeres‡ and C. L. Cooney§

*Departamento de Engenharia Quimica, Universidade Federal de Sao Carlos, SP, Via Washington Luiz km 235, 13.565-905 Sao Carlos, Brazil;

‡Centro de Engenharia Biologica e Quimica, Instituto Superior Tecnico, Lisboa, Portugal;

§Department of Chemical Engineering, Massachusetts Institute of Technology, Cambridge, MA, U.S.A.

(Received 1 December 1997, accepted 4 June 1998)

Abstract—This paper shows the results of flow visualization and residence time distribution experiments in a Taylor–Poiseuille vortex flow apparatus. It is the first of a series that starts with the identification of flow patterns inside the device and goes up to the assessment of its performance as an enzymatic reactor. Our approach is to study in depth one single geometric configuration (radius ratio $\eta = 0.677$ and aspect ratio $\Gamma = 18.30$), adequate for use as a heterogeneous reactor and/or adsorption system in bio-processes, rather than spanning a range of geometries and proposing empirical expressions for mass transport coefficients. The range of rotations and axial flow rates used here correspond to low/moderate rotational Reynolds numbers (Re_θ from 130 to 615, with $1.6 < Re_\theta/Re_{\theta,c} < 7.7$) and low axial ones ($Re_{ax}$ from 0.172 to 1.067). An unusual behavior of the system was noted in this operational region: the vortex drift velocities are less than one, and decrease continuously with increasing rotations, until a full stop. Except for Re_θ close to the critical value, the downstream displacement of vortices is slower than the mean axial velocity. The implications of this fact on the reactor performance are discussed.

Keywords: Vortex flow reactor; Taylor-Poiseuille flow; dispersion; mixing characteristics; flow patterns; residence time distribution.

1. INTRODUCTION

The objective of this communication is to outline some unusual characteristics of the Taylor–Poiseuille flow inside an apparatus that has geometric characteristics adequate for bio-process applications, as a heterogeneous bio-reactor or adsorption device.

The interest in using secondary vortex flow structures to improve the performance of chemical and biochemical reactors (usually known as vortex flow reactors, VFRs) has been periodically reported by several authors since the work of Kataoka *et al.* (1975). Figure 1 shows a schematic representation of a VFR.

For a heterogeneous solid–liquid system (for instance, a reactor with enzyme immobilized in gel beads) the VFR has the additional advantage of possessing one extra variable of operation: the rotation of the inner cylinder. It may be used to keep the particles in suspension for low axial flows—an otherwise difficult task in conventional fluidized-bed reactors. On the other hand, the agitation promoted by the inner cylinder is less aggressive than that one obtained with conventional stirrers, an important feature when sensitive particles, cells or large molecules are present in the medium.

From an operational point of view, the VFR should run, generally speaking, in a range of rotations where inter-vortex mixing is low. In this way, the VFR performance would get closer to a plug-flow reactor. From this point of view, the presence of wavy vortices (Coles, 1965) should be avoided, since waviness enhances inter-vortex mixing (see, for instance, the simulations reported by Ashwin *et al.*, 1995).

Many applied works in the field make the assumption that axial displacement of the vortices occurs in a stack form, with a drift velocity, V_d = ratio between the speed of the vortex center and the mean fluid axial velocity, close to unity. This flow pattern is named

†Corresponding author. E-mail: drcg@power.ufscar.br.

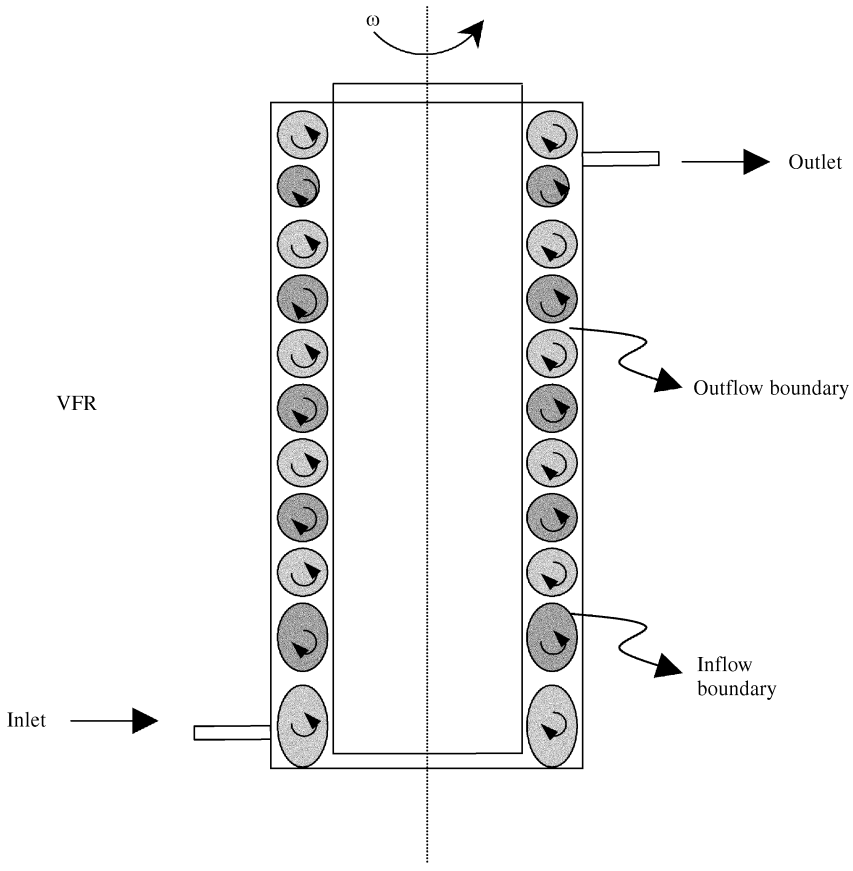

Fig. 1. Vortex flow reactor.

progressive Taylor vortices (PTV), and is one among the many possible stable states for this system (see, for instance, Lueptow *et al.*, 1992).

To simplify the flow pattern in a reactor in order to make the problem tractable is in the core of the chemical reaction engineering methodology. Nevertheless, the simple model should capture the main features of the flow if it is to be used in at least moderate extrapolations. For a VFR running in the PTV region, one of the important flow characteristics of the system is the relative speed of the vortices, the drift velocity V_d. If the hypothesis that V_d is close (or slightly greater than) unity is not correct for some combination of geometric factors, rotation and axial flow, a keystone of the classical simplified models for this situation may be affected.

The intent of this series of papers is to contribute to a deeper understanding of the behavior of VFR systems in the operational region of low axial flow, adequate for many bio-process applications. The usual chemical reaction engineering approach is applied here: first, identifying the main characteristics of the flow with the help of tracer experiments. Then, building-up a simplified model, able to simulate the reactor operation. Finally, validating the model against actual reaction data, after a careful assessment of the intrinsic and inherent kinetics and of the extra- and intra-particle mass transfer resistance. During these experiments an unexpected, stable and reproducible, flow pattern appeared which, to the best of our knowledge, has not been previously reported in the literature. Basically, the drift velocities measured in our apparatus are significantly less than one, and decrease with increasing rotation until the vortices stop moving downstream.

The experiments are conducted in an equipment with radius ratio ($\eta = R_i/R_o$) equal to 0.677 and aspect ratio ($\Gamma = L/d$) equal to 18.30. This geometry is chosen mainly for convenience, regarding our intention of using suspended particles in the gap, and to prevent the appearance of wavy vortices (Coles, 1965, refers that for $\eta < 0.714$ no wavy vortices are observed, for a system without axial flow).

In order to obtain reasonable conversions within the VFR, residence times between 30 and 120 min are used, leading to low axial Reynolds numbers ($Re_{ax} = U_{ax}.d/v$, between 0.172 and 1.067). Rotation rates are low, to avoid shear-mediated damage to the enzyme used in the reaction experiments. The rotational Reynolds numbers ($Re_\theta = \omega . R_i . d/v$) range spanned by the experiments goes from 130 to 615. It should be noted that the non-dimensional Taylor (Ta) number is more frequently used to describe rotation effects on this system. That is probably because it

appears naturally when the Navier–Stokes equations are put in dimensionless form. But that same reason is responsible for a number of different definitions for *Ta*, depending on the way each author formalizes the problem. For our purposes, this point is not relevant, and Re_θ replaces the Taylor number, without any loss of information.

Different inlet/outlet combinations are tested here to check the role of boundary conditions, but the main features of the flow are insensitive to these alterations. Different working fluids and tracers are used, and visualization experiments with suspended particles are also performed. All the experiments indicate the same flow pattern.

This paper presents these experimental results and discusses the implications of this behavior in the reactor performance. These results are placed in context through some relevant background information on Couette–Taylor and Couette–Taylor–Poiseuille (CTP) flows.

2. BACKGROUND

2.1. *The classical Taylor problem: no axial flow*

The secondary flow that appears above a critical rotation in the gap between an inner rotating and an outer cylinder (rotating or stationary) is probably one of the most widely studied phenomena in the field of fluid dynamics, ever since the remarkable work of Taylor (1923). This author discards the non-linear terms of the Navier–Stokes equations and solves these equations for the disturbances of the basic (Couette) flow using Bessel–Fourier series. In this way, it was possible to anticipate the critical rotation for the onset of instability, therefore extending Rayleigh's (1916) stability analysis of rotational flows to viscous incompressible fluids. The same paper shows experimental results in striking agreement with the theoretical predictions: above a critical rotation of the inner cylinder, counter-rotating toroidal vortices (now known as Taylor vortices) appear, superimposed to the main Couette flow. Furthermore, the actual size of the vortices agrees with theory. Chandrasekhar (1961) provides an excellent formalization of the linear approach for this problem.

Despite the number of published works in the literature, the understanding of the inherent complexities of this system is far from complete. Some topics still open to further study include: pattern selection among multiple solutions (for a theoretical non-linear approach of this subject see Chossat and Iooss, 1992), secondary instabilities (distinct modes of azimuthal wavy vortices, see the classical papers of Coles, 1964; Davey *et al*., 1968), and transition to turbulence (Barcilon *et al*., 1979; Koschmieder, 1979; Lathrop *et al*., 1992; Wei *et al*., 1992).

Many different stable states are visualized and mapped by Andereck *et al*. (1986), for a wide range of rotational Reynolds numbers in systems without axial flow. DiPrima and Swinney (1985) and Korschmieder (1993) present extensive reviews on closed Couette–Taylor systems. Tagg (1992) shows a list of around 1500 references concerning Taylor flow. Esser and Grossman (1996) have recently presented a simple analytical expression that accurately approximates the stability boundary in closed systems.

While Taylor's linear approach provides fairly good predictions of the onset of the vortices for cylinders of infinite length, it is inadequate when applied to supercritical flow, since the linear approximation incorrectly forecasts an exponential growth of the vortex size after the onset of the secondary Taylor flow. In the supercritical region, even for laminar flow, the non-linear terms of the Navier–Stokes equations should be considered. It is possible to solve these equations numerically; different techniques have been presented for this purpose [see, for instance, Marcus (1984a, b) for an interesting approach using a spectral method adequate also for non-axisymmetric problems like wavy vortices].

Alternatively, one may resort to the weakly non-linear theory, which decouples time and spatial dependence in the solution for the velocities (the so-called shape assumption). The ordinary-differential equation that describes the time- dependence of the amplitudes of the disturbances of the velocity field is called the Ginzburg–Landau equation, and its parameters are related to the eigenvalues of the infinite series solution for the velocity profile (see Davey, 1962; DiPrima and Swinney, 1985).

2.2. *Couette–Taylor–Poiseuille flow*

The superposition of an axial Poiseuille annular flow to the Couette–Taylor system increases the complexity of the problem: several different spatiotemporal stable states may appear in the Couette–Taylor–Poiseuille (CTP) flow. Chandrasekhar (1961) predicts, based on the linear theory, that the axial flow would have a stabilizing effect, delaying the formation of the vortices up to higher rotations. This fact is experimentally observed by Snyder (1962) for axial Reynolds numbers up to 100, in an apparatus with radius ratio (η) equal to 0.95. This author also confirms the linear theory prediction of a drift velocity (V_d) close to 1.2. Nevertheless, for higher Re_{ax} (above 6000), the instability of the axial Poiseuille flow becomes dominant, and an increase in Re_{ax} would destabilize the flow in this region (Takeuchi and Jankovski, 1981; Ng and Turner, 1982; Stuart, 1986).

In a series of papers, Gu and Fahidy (1985a, b, 1986) report results of visualization experiments with injection of dye, for a wide range of rotational Re_θ and Re_{ax}, and different geometric factors, Γ and η. They identify several flow regimes: propagating Taylor vortices, inclined propagating vortices, wavy and modulated wavy propagating vortices. Takeuchi and Jankovski (1981) had already observed the first two regimes. Lueptow *et al*. (1992) used particles in visualization experiments and perform a spectral analysis of reflected laser light, with an apparatus having $\eta = 0.848$ and $\Gamma = 41$. Their range of measurements is

0–37 for Re_{ax} and 0–2900 for Re_{θ}. In this region they observe seven different regimes with propagating Taylor vortices, from a total of 12 regimes, ranging from spiral flow to laminar Couette–Poiseuille flow.

Tsameret and Steinberg (1994a) study the onset of the instability for the low Re_{ax} region (0–4) with $\eta = 0.707$ and 0.770, $\Gamma = 54$ and 48, using a laser-Doppler anemometer. They observe that propagating Taylor vortices may occur either in an absolutely unstable region, where the disturbance can propagate upstream, or in a convectively unstable mode, where the disturbance is 'washed out' of the system. In any case, the axial flow rate and boundary conditions exclusively define the amplitude of the vortices. The same authors afterwards expand their Re_{ax} range up to 15, and observe the onset of other stable states, stationary spirals and moving spirals (Tsameret and Steinberg, 1994b).

It may be interesting for our purpose here to briefly illustrate how a spectral analysis of the solution for the velocity disturbances permits the prediction of the drift velocity V_d. This approach uses a series solution for the disturbances, with the following formulation:

$$v_j' = f(r')e^{i(kz' + m\theta) + (\sigma - i\omega)t'} + \text{c.c.} \quad (1)$$

Here, v_j' is the disturbance from the basic flow for the component j of the velocity field: $v_j' = v_j - v_{j,\,\text{Couette}} - v_{j,\text{Poiseuille}}$ [following Chandrasekhar (1961), the basic stable flow is a linear combination of rotational Couette flow and annular, axial, Poiseiulle flow]. In (1), the independent variables are dimensionless (usually, $r' = r/d$; $z' = z/d$; $t' = tv/d^2$). The mode k is the wave number in the axial direction ($k = 2\pi/\lambda$, where $\lambda =$ height of a pair of counter-rotating vortices), m is associated with the number of waves in the tangential direction, σ is the exponential growth rate of the perturbation, and ω is the oscillation frequency of the solution.

The system is stable if $\sigma < 0$ for all the (infinite) modes of the disturbance represented by eq. (1). The marginal (or neutral) stability boundary of the system corresponds to $\sigma = 0$, and is the limit for the onset of the instability. The system boundary conditions, together with the imposition of non-trivial solutions for v', will lead to an eigenvalue problem that, once solved, gives the values of σ and ω. The CTP problem will have an oscillatory solution, since the toroidal (or spiral) vortices are expected to travel downstream. In this case, the imaginary part ω will be non-zero for $\sigma = 0$ (on the onset of instability). For the pure Couette–Taylor problem, without axial flow, both σ and ω are equal to zero.

If the flow is axisymmetric (without waviness or spirals), $m = 0$ and $V_d = \omega/(kRe_{ax})$. Ng and Turner (1982) determine the critical modes k, m, σ and ω in a wide range of Re_{ax} (0–6000). In both cases, they obtain V_d essentially equal to 1.17, when $Re_{ax} < 10$ ($\eta = 0.95$, for axisymmetric disturbances, and $\eta = 0.77$, for non-axisymmetric ones).

Recktenwald *et al.* (1993) solve the Ginzburg-Landau (GL) equation for the CTP flow with Re_{ax} up to 20 and η from 0.1 to 0.975 and predict the critical Re_{θ} ($Re_{\theta,c}$) for the onset of instability. They present relationships for the critical values (at the onset of the instability) of k and ω. Using these values, their computed V_d would range from approximately 1.27–1.17, for small values of Re_{ax} and $0.1 < \eta < 0.975$.

Büchel *et al.* (1996) compare the Navier–Stokes (solved with a time-dependent finite-differences algorithm) and the Ginzbunrg–Landau predictions for the absolutely unstable regime with $Re_{ax} < 4$, and notice that the structure of the propagating vortices is independent of the parameters history and system initial conditions.

One is led to conclude from the observations made before, that there are a variety of possible stable states, even if the analysis is restricted to PTV flows. The axial flux seems to stabilize the system to a certain degree, inhibiting some bifurcations that are present in the closed Taylor device (mainly with respect to multiplicity of vortex wavelengths). Nevertheless, the unfolding of different patterns is still considerable.

2.3. *The applied approach*: *vortex flow reactors*

When one is concerned with simulating chemical and biochemical processes, which usually include mass transfer resistance and complex kinetics, not all the theoretical background can be used, or else the mathematical model would not be feasible to applications such as reactor design/scale-up and process optimization and control. It is necessary to rely on a simplified flow model, and on empirical equations for the mass transfer coefficients (which nevertheless must be consistent with the assumptions of the model).

Some attempts have been made towards using theoretical velocity profiles, derived from the linear or weakly non-linear theory, in the mathematical modeling of VFRs. The trade-off in this approach is that its limits of applicability are essentially narrow. Kataoka (1975) follows the approach of Stuart (1958) and Davey (1962) to derive the equilibrium amplitude of the vortex velocities and from them, calculate heat transfer coefficients to the cylinder walls. Cohen and Maron (1991) use the same approach to generate velocity profiles, and then solve mass balances for a generic consecutive reaction scheme, neglecting inter-vortex mass transport. Both works (Kataoka, 1975; Cohen and Maron, 1991) actually resort to solutions for the velocity field inside a closed Taylor system (without axial flow), and make the 'stack of vortices' assumption ($V_d = 1$) in order to describe the axial movement.

Haim and Pismen (1994) use a linear simplification of the Navier–Stokes equations for the complete CTP problem to model a photochemical reactor. Differently from other works, the authors do not simplify the flow pattern to a stack of vortices, but take in account a 'slalom' by-pass around them. Nevertheless, the

linear theory cannot predict amplitudes and drift velocities of the vortices; the authors present a series of sensitivity tests, assuming $V_d = 1.17$ and using the vortex amplitude as a parameter.

VFR experimental results with the presence of a reaction are less abundant in the literature. Two recent examples can be cited: Sczechowski *et al.* (1995), for a photocatalysis reactor and Kataoka *et al.* (1995) for a polymerization reactor.

On the other hand, several works present VFR mass transfer experiments. For the sake of conciseness, only the main aspects of the problem are summarized here. Kataoka's group (see, for instance, Kataoka and Takigawa, 1981; Ohmura *et al.*, 1997) use the stack assumption ($V_d = 1.0$) and adopt a well-mixed two-vortices set as the basic model cell. The basis for that assumption is that the slow inflow inter-vortex boundary (where the radial component of the velocity is directed towards the inner cylinder) offers significant resistance to mass transfer, while the fast outflow boundary is not a considerable barrier. Kataoka and Takigawa (1981), present an expression for the inter-(pair of)-vortices mass transfer coefficient, as a function of Re_{ax} and of the molecular diffusivity.

Legrand and Coeuret (1986) also use the 'stack of vortices' general approach, but stress that the intra-vortex tangential dispersion is low in the laminar region (see also Legrand *et al.*, 1983; Legrand and Coeuret, 1987).

Pudjiono *et al.* (1992), Pudjiono and Tavare (1993) and Moore and Cooney (1995) apply the classical axial dispersion model to this problem, covering a broad range of Re_θ and Re_{ax}. In this approach, the detailed vortex structure is not important. Tam and Swinney (1987) use the same model, but restricted to the turbulent region.

If one admits that an adequate reactor feed may solve, at least to a first approximation, the contradiction between the well-mixed vortex models and the ones that stress the importance of tangential dispersion, all the previous works would have a common feature. That is: a one-parameter mass transport model would essentially suffice to describe the system.

Desmet *et al.* (1996a, b) present another point of view: the vortices would not be well mixed, especially in the laminar region. They disregard differences between inflow and outflow boundaries (so their basic cell is a single vortex) and model the intra-vortex dispersion using two concentric well-mixed zones. In this way, their model has, in the laminar region, two parameters: the inter- and intra-vortex mass transfer coefficients. Changing the point of injection of tracer, they show experimental evidence in support of the two-zone model: injections close to the outer cylinder wall would quickly by-pass the vortices, since the inter-vortex mass transfer coefficient would be higher than the intra-vortex one for low rotations. In two subsequent papers (Desmet *et al.*, 1997a,b) improvements in the experimental set-up allow the authors to analyze transient effects and to model inter- and intra-vortices dispersion. Nevertheless, all their experiments are performed in a closed system (without axial flow). Their insight on the vortex structure shows that slow intra-vortex mixing may increase the effect of tracer injection conditions on the system response, during residence time distribution (RTD) experiments. But in order to quantitatively apply their mass transfer expressions to the simulation of the VFR, it is necessary to rely on the 'stack of vortices' approach. More recently, Campero and Vigil (1997) use the same approach and propose a three-parameter model, to take in account non-ideal mixing in the inner vortex region of Desmet *et al.* (1996a, b).

It should be noted that extrapolation of quantitative results from an apparatus without axial flow to a continuous VFR must be made carefully. For instance, the simulations made by Haim and Pismen (1995) and Lueptow and Hajiloo (1995) clearly show the possible existence of a by-pass convective flow around the vortices. And the experimental results presented in this work contradict the 'stack assumption' for the reactor geometry and the range of rotations and axial flows studied here.

3. EXPERIMENTAL

Dimensions and geometric characteristics of the system used in this work are constrained by the demands of its application as a heterogeneous enzymatic reactor. In some flow visualization and tracer injection experiments, a jacketed reactor is used, but most of the results shown are obtained at room temperature ($22 \pm 1^\circ$C) with the experimental set-up depicted in Fig. 2. The external stationary cylinder is made of acrylic, and the inner (rotational) one of polypropylene. A stainless-steel shaft is positioned throughout the inner cylinder, to increase the system inertia and reduce wobbling. Rotation is provided by a magnetic drive, adapted from Membrex (Fairfield, NJ) Benchmark filtration equipment, controlled by an Electro-Craft E625-M unit and measured with a Metron tachometer.

The apparatus design is determined by one important restriction that arises when it is used as a heterogeneous VFR: shear-sensitive particles should suffer a minimum damage in long-run experiments. One of

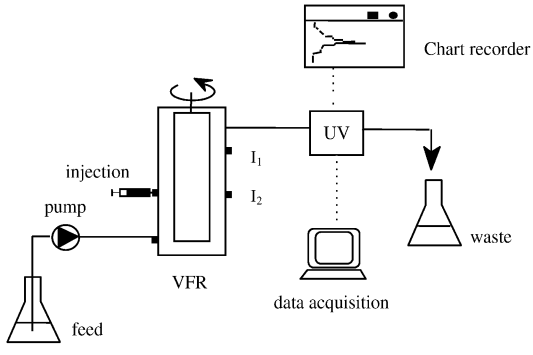

Fig. 2. Experimental set-up.

the important causes of particle destruction may be the friction between moving and stationary parts of the equipment (seals and bearings). To check this point out, several long-run tests (from 4 h to 2 days, with rotations from 200 to 2000 rpm) were made, with particles that present regular, spherical shape. Using Sephacryl S-1000 ($\phi_{av} = 50\ \mu$m) and Streamline (base matrix, $\phi_{av} = 150\ \mu$m), from Pharmacia, a range of particle relative densities from 1.05 to 1.30 could be covered. After each run, particle integrity was assessed, with the aid of an optical microscope. After a series of tests with different configurations, one is selected as the less aggressive for the particles: the bottom bearing of the inner cylinder is eliminated, keeping it in balance, within a distance of about 1 mm from the bottom wall. The outlet is positioned at the outer cylinder wall, below the top of the apparatus (see Fig. 2). In this way, fluid and particles have no contact with moving seals. It should be stressed that the rotation of the top and bottom vortices always impels the particles towards the seals. If the end walls of the device are stationary, the adjacent vortex layer moves towards the inner cylinder, dragging the particles to the friction zone (the seal between the inner cylinder and the stationary wall). If a moving wall is used, attached to the inner cylinder, the particles will be dragged towards the outer wall, and against the seal. This behavior of the boundary vortices was observed in our device, and agrees with the literature (Koschmieder, 1993).

A drawback of this design is that the absence of the bottom bearing slightly increases the internal cylinder wobbling. Nevertheless, at least for the rotation rates used in this study (15–400 rpm), this movement is not excessive, and the high reproducibility of the experiments (made with two different sets of cylinders) indicates that the results are consistent.

The VFR uses two different outlets: one at the side of the external cylinder ($\phi \approx 2$ mm); in this case, compressed air keeps the fluid level constant for different axial flow rates. Alternatively, the fluid exits through an orifice ($\phi \approx 3$ mm) at the top of the device (the usual Membrex retentate exit). Two different inlets are tested: a lateral orifice on the wall of the outer cylinder ($\phi \approx 2$ mm), and a tube reaching the middle of the annular gap ($\phi \approx 1.5$ mm). Dimensions and operational conditions are described in Table 1. The vortex flow apparatus has $\eta = 0.677$ and $\Gamma = 18.30$.

Different working fluids are employed in the experiments: water (distilled, deionized), glycerol–water mixtures up to 4.2 M in glycerol ($\mu = 3.00 \times 10^{-3}$ kg/m s at 22°C), glucose–water and fructose–water solutions (ranging from 0.5 M to 5 M; a 2 M glucose/water solution presents $\mu = 2.82 \times 10^{-3}$ kg/m s). The experimental set-up spans the range of dimensionless numbers: Re_{ax} 0.172–1.067 and Re_θ 130–615.

In residence time distribution (RTD) experiments, outlet tracer concentrations are measured with a continuous flow UV detector using a 280 nm filter (Pharmacia). The output signal (mV) is sent to a PC computer, using a Paragon data acquisition/control system (Intec Controls Corp.), and a paper backup chart is made in a x-time register. A chromatography syringe is used for tracer injections, through orifices 3.16 and 9.04 cm distant from the top level of the fluid inside the apparatus (see Fig. 2). Alternatively, a four-way chromatography valve is used for this purpose. In both cases, the injected volume is 160 μl. Two tracers with very different molecular sizes are employed, to verify if diffusion affects the RTD. Alizarin red S, Eastman Org., molecular weight 326 ($D_M = 7.5 \times 10^{-10}$ m^2/s at 22°C, infinite dilution in water), and blue dextran, Sigma, average molecular weight 2×10^6 ($D_M = 8.0 \times 10^{-12}$ m^2/s at 22°C, infinite dilution in water). To obtain a linear response from the UV detector, the concentration of tracer in the injection sample is fixed at 2 g/l (alizarin red) and 5 g/l (blue dextran). The outlet tubing inner diameter is ≈ 1 mm, and less than 30 mm long; the exit hold-up volume is less than 0.02% of the VFR annular volume.

Table 1. Vortex flow reactor dimensions and operational conditions

Dimensions:	*Operational conditions*:
Inner cylinder radius 1.71×10^{-2} m	Inner cylinder rotation rate, 0–21 s^{-1}
Outer cylinder inner wall radius, 2.53×10^{-2} m	Axial flow rate, 0–1.4×10^{-7} m^3/s
Total height, 1.73×10^{-1} m	Re_θ range, 130–615
Wet region height, 1.49×10^{-1} m	Re_{ax} range, 0.172–1.067

Visualization experiments are made with a 0.5% (v/v) suspension of Kalliroscope AQ-1000, Kalliroscope Corp. Other particles are also tested: beads of Sephacryl S-300, Pharmacia; and Maxazyme, Gist–Brocade, gel particles with immobilized glucoisomerase previously ground and sieved ($\phi_{av} = 250\ \mu$m). The last one is the catalyst that will be employed in reaction experiments. A Cole–Parmer peristaltic pump provides the axial flow.

Either for the visualization with particles or in tracer experiments, it is possible to visually follow the displacement of the vortices. The position of the vortex boundaries is measured with a caliper, and their velocities calculated after plotting their axial position versus time.

4. RESULTS AND DISCUSSION

RTD experiments start with a careful injection of different tracers through the external cylinder wall. Since it is not possible to know the vortex position beforehand, different regions are reached by chance: the center of a vortex (with an outflow or an inflow upper boundary), or the by-pass region between successive vortices. The acrylic cylinder allows a clear visualization of the tracer progression and by changing the needle position it is possible to inject close to the walls or in the middle of the gap. A series of replicates is made for each operational condition.

Figure 3 depicts a typical set of results for a series of injections in the vortex center.

These profiles are obtained using a side outlet and with injections through point I1 (see Fig. 2). The inlet flow comes through the wall of the external cylinder.

A qualitative analysis of these responses indicates that the reactor changes from an almost plug-flow behavior at $2.72\,s^{-1}$ (26 rpm) to a characteristically high-dispersion, well-mixed reactor profile at $7.85\,s^{-1}$ (75 rpm). All the discontinuities in the slope of the curves that appear below $5.64\,s^{-1}$ are due to the collapse of the vortices at the top of the apparatus, which generate end effects that are registered by the UV unit. There is a shift of the peak correspondent to the vortex labeled by the tracer: it leaves the reactor at higher times for increasing rotations. At $5.97\,s^{-1}$ this peak is detected after ≈ 7000 s, and above this point the response curve becomes smooth. Runs up to 18,000 s confirm the absence of any sharp peak (see Fig. 3, for $7.85\,s^{-1}$).

Figure 4 shows more clearly the responses corresponding to 2.72 and $7.85\,s^{-1}$ for the same experiment, illustrating two extreme behaviors.

The intervals between valleys in the $2.72\,s^{-1}$ curve correspond to the time spanned between collapses of successive vortices. When the vortices are moving, they collapse periodically at the top of the VFR. Visual observations indicate that the penultimate vortex gradually shrinks down to a critical size. It collapses at this point, mixing its contents with the two contiguous (upper and lower) vortices. Figure 5 illustrates these phenomena.

If a vortex that has received an injection of tracer has an upper boundary directed inwards there is a delay in its collapse. On the opposite, if this vortex presents an outflow upper boundary, it is less stable, and a sudden collapse occurs, instead of a gradual shrinking (see Fig. 5). The spike pattern of some of the RTD curves is due to this shrinking-collapse-dilution end effect. The sharp edges of the spikes correspond to the collapse of the penultimate vortex. Figure 6 shows how the RTD curve reflects these end effects.

Both curves in Fig. 6 are remarkably reproducible. They depict the difference between slow inflow and fast outflow vortex boundaries. These results are for a side outlet reactor configuration: inflow boundaries are more stable, delaying the top vortices' collapse until the penultimate vortex has its size considerably reduced. The higher radial momentum associated to the outflow boundary, on its turn, is responsible for a rapid disruption of the vortex structure when it approaches the exit, resulting in the sharp slope apparent in the figure. A simplified model of the flow through the VFR must consider these phenomena and filter their interference on the mass transfer parameters fitting procedure. Figure 7 compares RTD curves for two different VFR outlet configurations, and again the influence of end effects is clear.

It can be seen in Fig. 7 that the periodicity of the collapse of the vortices does not change when the top boundary condition is altered from a side outlet, perpendicular to the cylinder wall, to a top outlet, perpendicular to the liquid level.

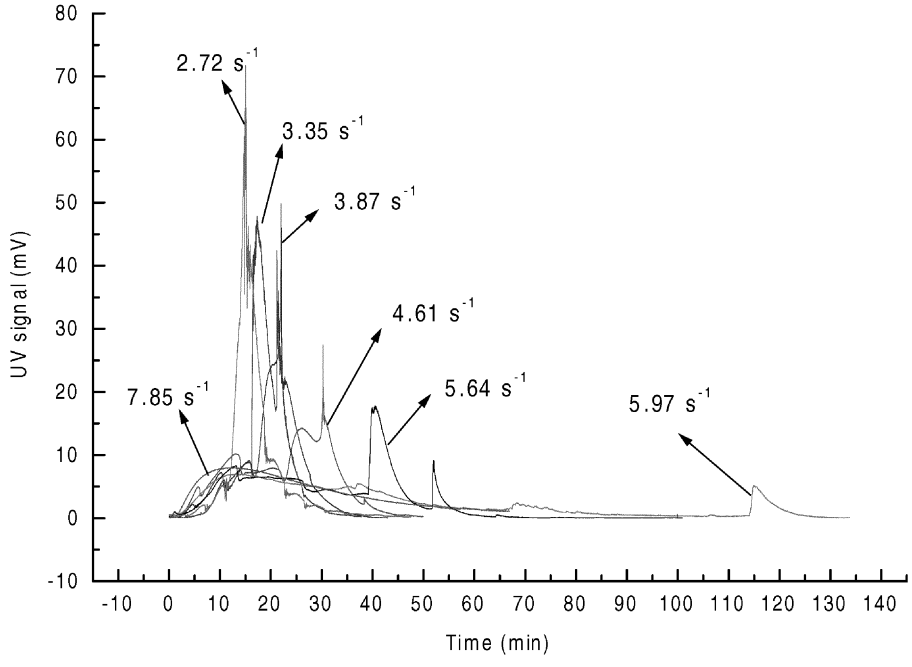

Fig. 3. VFR residence time distributions for different rotation rates of the inner cylinder. Fluid: glycerol/water solution, 4.2 M glycerol, $\mu = 3.0 \times 10^{-3}$ kg/(m s). Tracer. blue dextran, $D_M = 3.0 \times 10^{-12}$ m^2/s. Axial flow rate: 7.67×10^{-8} m^3/s. $T = 22°C$.

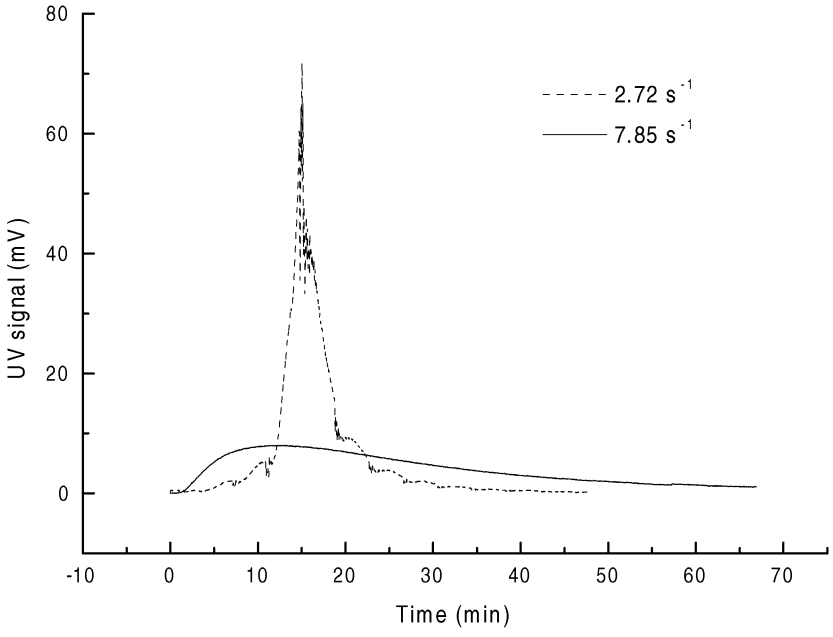

Fig. 4. VFR residence time distributions. Fluid: glycerol/water solution, 4.2 M glycerol, $\mu = 3.0 \times 10^{-3}$ kg/(m.s). Tracer: blue dextran, $D_M = 3.0 \times 10^{-12}$ m^2/s. Axial flow rate: 7.67×10^{-8} m^3/s. $T = 22°$C.

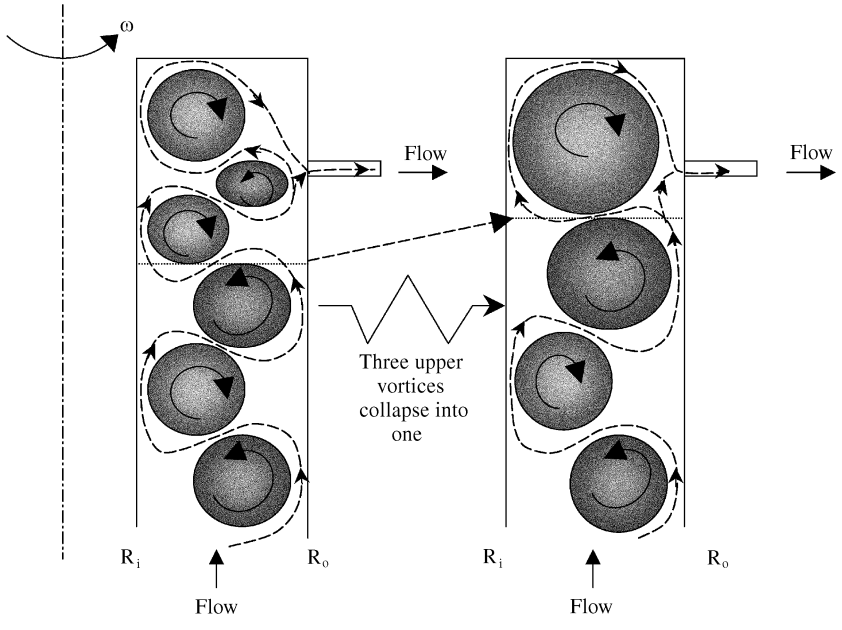

Fig. 5. Schematic representation of the top vortices' collapse at the reactor outlet. The upper vortex displays an inflow (stable) lower boundary. Dashed lines represent the by-pass flow.

Several tests are performed to verify the influence of start-up conditions on the flow pattern. Assays with sudden start-ups and using ramps for the rotation rate, with different slopes (in both directions, clockwise and counterclockwise), are compared. The responses, for all cases, are systematically equal. In the range of variables tested therein, there is no sign of multiple steady states. Figure 8 is an example of these results.

Figure 9 consolidates some results for different tracer-fluid combinations. The (main) peak height is chosen to identify the transition between a plug-flow and a well-mixed behavior. Even though a plot of peak height versus rotation rate, for a fixed axial flow,

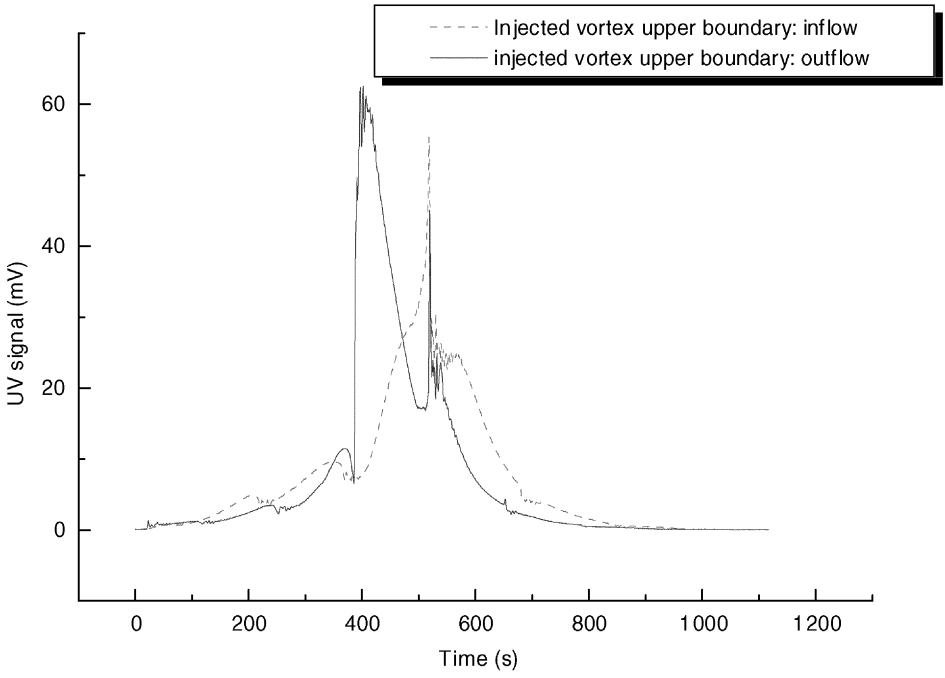

Fig. 6. VFR residence time distributions. Injection at distinct vortices. Glycerol/water, 4.2 M, $\mu = 3.0 \times 10^{-3}$ kg/(m s). Tracer: blue dextran, $D_M = 3.0 \times 10^{-12}$ m^2/s. Axial flow rate: 1.67×10^{-7} m^3/s. Rotation rate: 4.71 s^{-1}. $T = 22°$C.

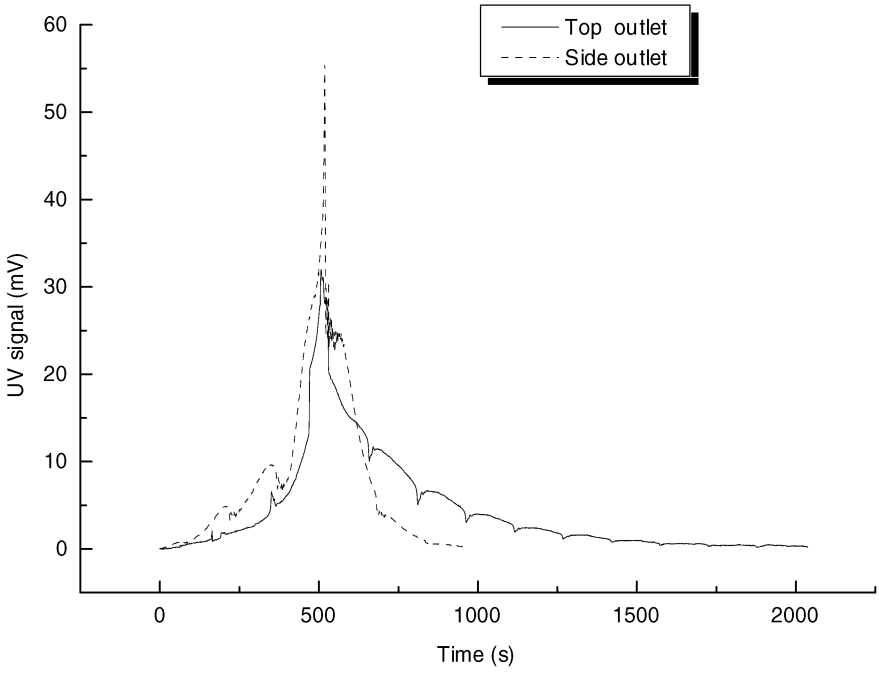

Fig. 7. VFR residence time distributions. Different outlet positions. Glycerol/water, 4.2 M, $\mu = 3.0 \times 10^{-3}$ kg/(m s). Tracer: blue dextran, $D_M = 3.0 \times 10^{-12}$ m^2/s. Axial flow rate: 1.67×10^{-7} m^3/s. Rotation rate: 4.71 s^{-1}. $T = 22°$C.

may show a minimum (close to the perfectly mixed CSTR limit, see Fig. 3), this parameter is still useful to our present discussion.

All the experimental data show a similar behavior, with a transition zone between plug-flow and perfectly mixed patterns. For lower feed rates, the axial dispersion decreases the peak heights (see water/blue dextran, $Re_{ax} = 0.173$ in Fig. 9) but the basic trend is the same. Figure 10 shows results for different axial flows, using the same fluid/tracer combination. The

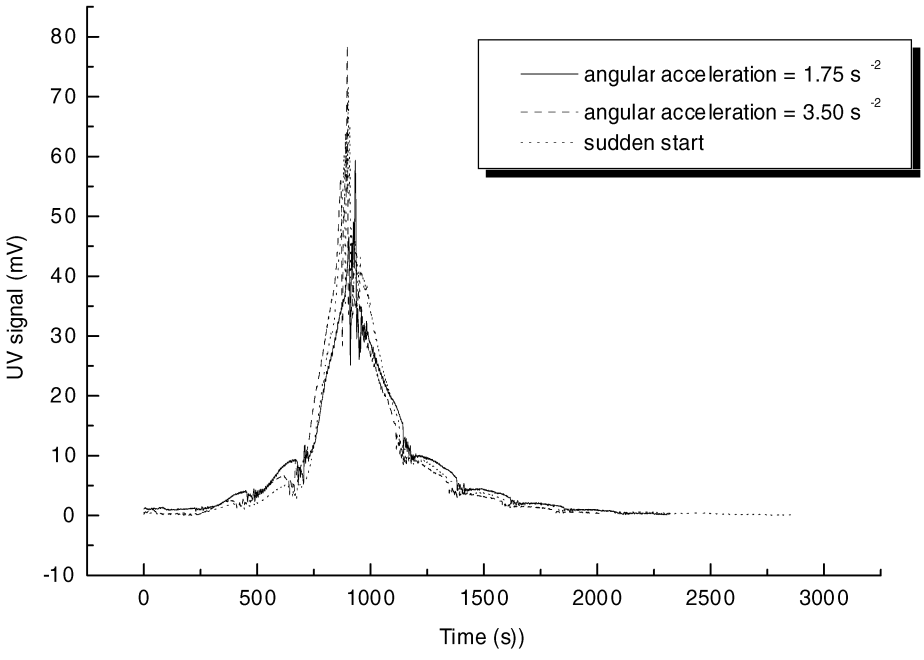

Fig. 8. VFR residence time distributions. Different start-up conditions. Glycerol/water, 4.2 M, $\mu = 3.0 \times 10^{-3}$ kg/(m s). Tracer: blue dextran, $D_M = 3.0 \times 10^{-12}$ m^2/s. Axial flow rate: 7.67×10^{-8} m^3/s, Steady state rotation rate: 2.56 s^{-1}. $T = 22°$C.

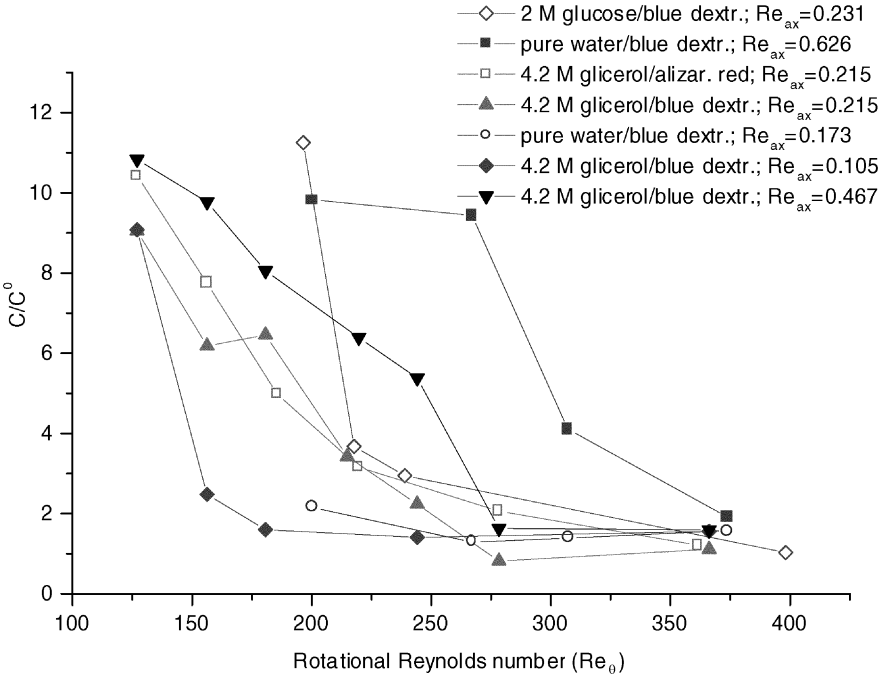

Fig. 9. VFR residence time distributions: dimensionless peak heights. $T = 22°$C.

region of transition plug-flow/well-mixed-reactor is not large.

Desmet *et al.* (1996a, b) also report a sharp transition in their experiments, justified as a result of the onset of turbulence. Ohmura *et al.* (1997), on the other hand, do not detect any sharp discontinuity in the axial dispersion coefficient. The experiments of both groups are made in closed systems, without axial flow. One point that may arise is if the behavior described beforehand is due to turbulent effects or to

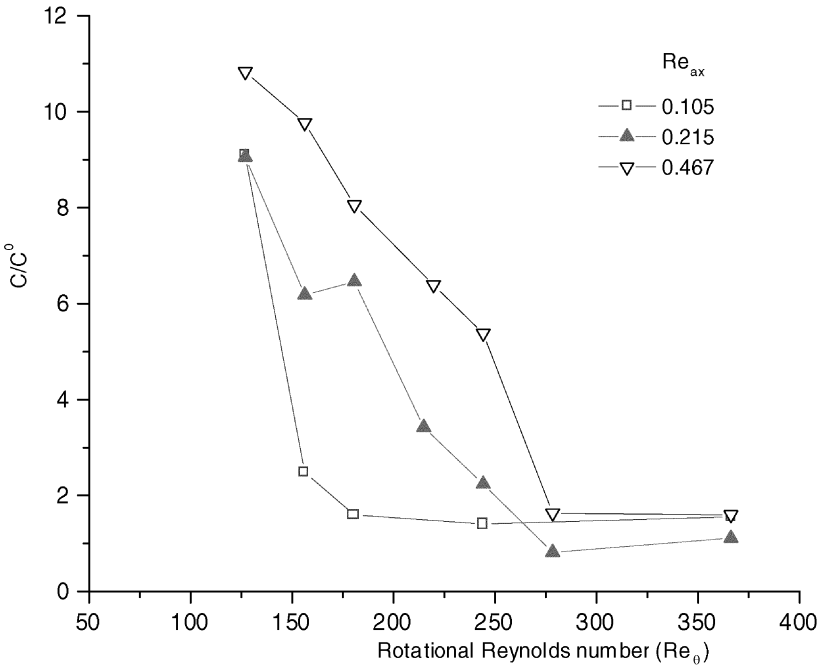

Fig. 10. VFR residence time distributions: dimensionless peak heights. Glycerol/water, 4.2 M, $\mu = 3.0 \times 10^{-3}$ kg/(m s). Tracer: blue dextran, $D_M = 3.0 \times 10^{-12}$ m^2/s. $T = 22^\circ$C.

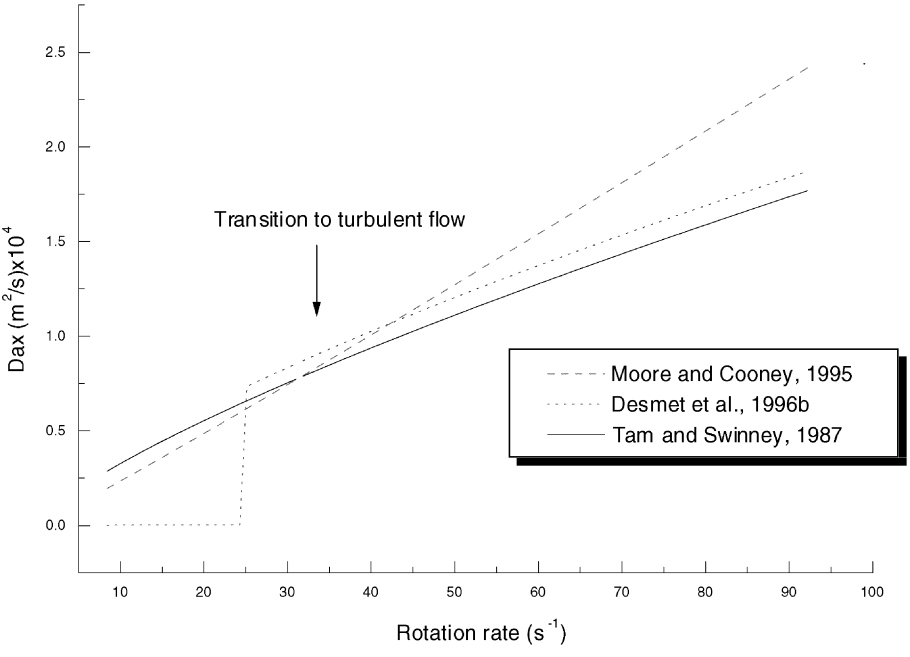

Fig. 11. VFR axial dispersion coefficients (D_{ax}), calculated from the literature. Fluid: water, 22°C.

the starting of wavy vortices. It should be stressed that in all the runs performed here, a visual observation of the vortex pattern does not show any sign of waviness. For tracer experiments as well as for visualization runs using Kalliroscope and Maxazyme gel particles, the flow pattern always corresponds to the PTV regime.

To illustrate the role that turbulence can play, some calculations of the axial dispersion are made using the expressions of Desmet *et al.* (1996b) (with $D_{ax} = K_{intervortex} \cdot d$). The results are compared with Tam and Swinney's (1987), (extrapolated in the laminar region) and Moore and Cooney's (1995) for the axial dispersion coefficient (Fig. 11).

The curves in Fig. 11 are for the water/blue dextran system. The transition to turbulent vortices indicated in that figure actually corresponds to an average of the results reported in Di Prima and Swinney's (1985) review for an apparatus with $\eta \approx 0.875$, without axial flow. The arrow in Fig. 11, therefore, is a qualitative indicator of the center of the region where turbulent noise should begin to be noticed.

For the geometry studied here, nevertheless, the beginning of turbulence would be at a rotation rate one order of magnitude greater than the transition range in Figs 9 and 10. The visualization of tracer injections also corroborates the conclusion that the transition occurs in the region of laminar flow. The dye dispersion is slow, even when the VFR's RTD has a smooth shape (see, for instance, the $7.85\ s^{-1}$ rotation rate curve in Fig. 3). Although the tracer seems to be well mixed in the vortex when it reaches the reactor outlet, it takes some minutes before the whole vortex is homogeneously filled, and it is possible to follow the streaklines during this period. This qualitative observations agree with the idea that intra-vortex mixing in the laminar region is slow (following Legrand, J. and Coeuret, F., 1986), but also corroborate the conclusion that the transition observed here is not due to turbulence.

In order to verify the role of intra-vortex diffusion, it is useful to define (following Pudjiono *et al.*, 1992) the dimensionless quantity τ, ratio of the characteristic time for convection to that for intra-vortex diffusion, $\tau = L \,.\, D_M/(U_{ax} \,.\, d^2)$. For the experimental set-up used in this work, τ ranged between 4×10^{-5} (blue dextran/glicerol, $U_{ax} = 1.54 \times 10^{-4}$ m/s) and 8×10^{-2} (alizarin red/water, $U_{ax} = 2.05 \times 10^{-5}$ m/s). Therefore, the region covered by the experiments includes both strong and weak diffusional effects. Nevertheless, system responses are essentially the same in all the experiments, despite of the value of τ. It should also be stressed that the manual injection of tracer permits a fine control of the distribution of dye along the azimuthal direction of the vortex. These facts come in support to the hypothesis that the main characteristics of the RTD curves are not due to intra-vortex diffusion.

Figure 12 displays the results of a sensitivity analysis using the flow models and mass transfer coefficients of Desmet *et al.* (1996b) and Moore and Cooney (1995). The working fluid is water and the tracer, blue dextran.

Curves 1–3 in Fig. 12 are obtained using the approach suggested by Desmet *et al.* (1996a): mass balances for the two regions that constitute the vortices are solved. The stack of vortices translates along the reactor length, and when a new vortex enter the system, the last one disappears. At the reactor exit, the concentration is taken as the radial average in the last vortex. The resulting set of ordinary differential equations is solved using the algorithm DASSL, Brenan *et al.* (1989). Curve number 4 (Moore and Cooney, 1995) is obtained after the solution of the mass balance equation, considering the axial dispersion term — a classical two-point boundary value transient problem. This partial differential equation is solved through the method of lines: the spatial variable (axial length) is discretized (using spline orthogonal collocation, Villadsen and Michelsen, 1978), and the resulting set

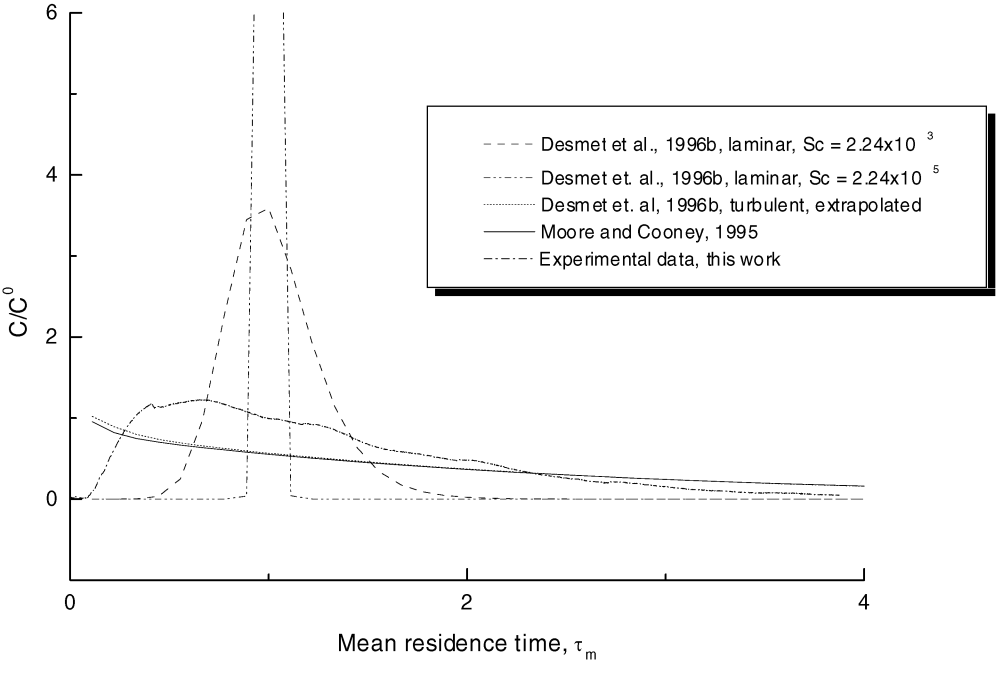

Fig. 12. VFR responses for a pulse of tracer, calculated from the literature. Water, 22°C. Tracer: blue dextran, $D_M = 8.0 \times 10^{-12}\ m^2/s$. Axial flow rate: $4.17 \times 10^{-8}\ m^3/s$. Rotation rate: $3.35\ s^{-1}$.

of ordinary differential equations, having time as independent variable, is solved numerically (with the algorithm DASSL). The importance of an adequate flow model to correctly forecast the behavior of this system is evident from these results. The fitting to the experimental data could be improved, of course, by changing model parameters, but the main question is: do the stack of vortices or the classical axial dispersion models suffice to capture the main features of the flow, at least for the situation described in this work?

The cause of the VFR behavior observed here becomes clear when drift velocities (V_d) are computed. The shift of peaks observed in Fig. 3 is by itself an indication that increasing rotations delay the vortices downstream movement; this trend is confirmed by the data presented in Figs 13a–c.

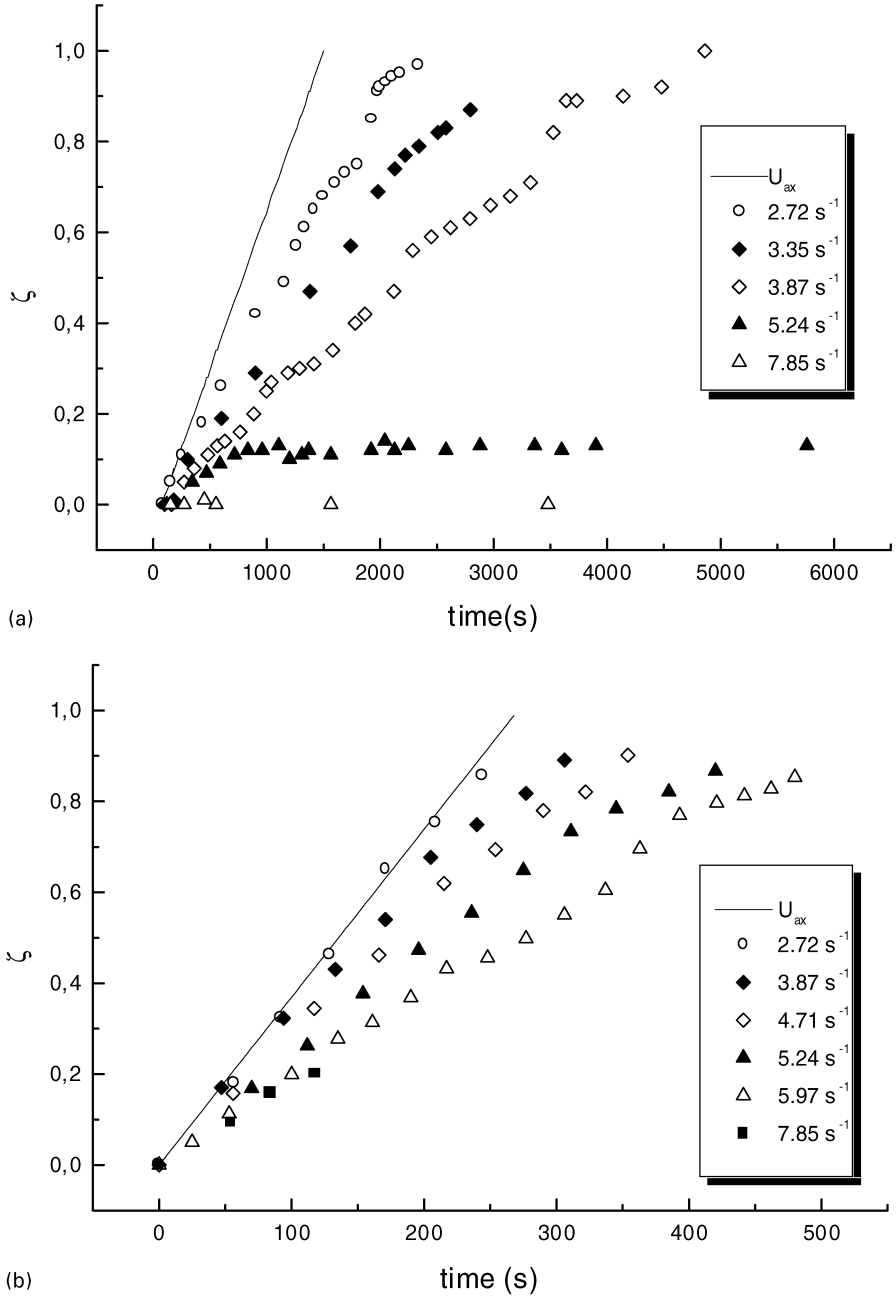

Fig. 13. Downstream vortex displacement for different rotation rates. (a) Axial flow rate: 4.58×10^{-8} m^3/s. Glycerol/water, 4.2 M, $\mu = 3.0 \times 10^{-3}$ kg/(m s). Tracer: blue dextran, $D_M = 3.0 \times 10^{-12}$ m^2/s. $T = 22°$C. (b) Axial flow rate: 1.67×10^{-7} m^3/s. Glycerol/water, 4.2 M. Tracer: blue dextran. $T = 22°$C. (c) Downstream vortex displacement for different rotation rates and injection positions. Axial flow rate: 7.67×10^{-8} m^3/s. Glycerol/water, 4.2 M. Tracer: blue dextran. $T = 22°$C.

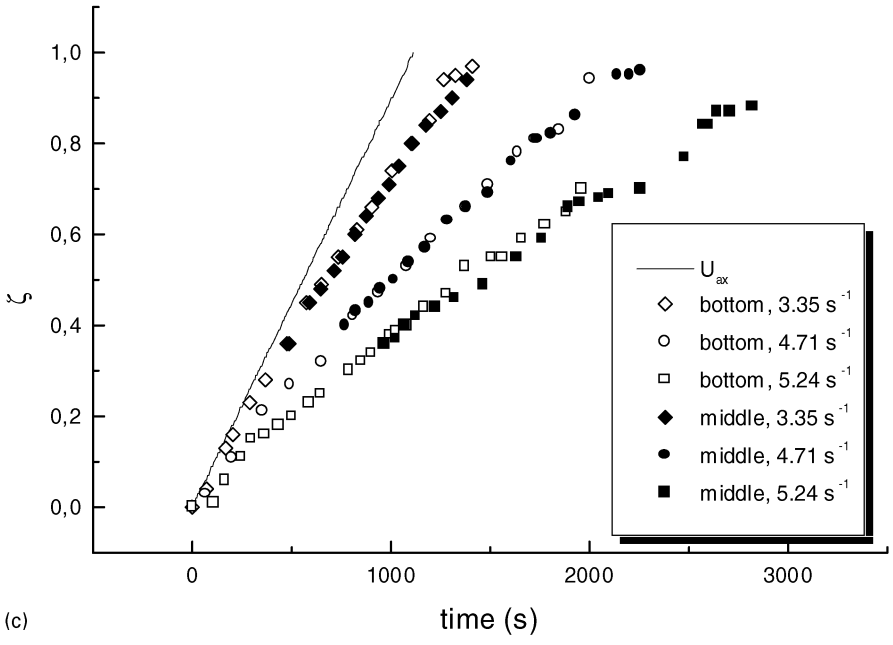

Fig. 13. *Continued.*

The sequence of Figs 13a–c is a typical collection of empirical results, for one fluid/tracer combination. It is clear that increasing axial flows tend to bring the curves for different rotations closer, and, on the other hand, increasing rotation rates of the inner cylinder tend to stop the axial displacement of the vortices. When $V_d \to 0$, all the net axial flow through the VFR will occur through a by-pass around the Taylor vortices. Figure 13c exemplifies the accuracy of the measurements, comparing results obtained for different points of injection of tracer. End effects are responsible for a decrease in V_d when the vortex approaches the reactor outlet. It is evident from these results that a strong deviation from a perfectly stacked flow pattern occurs. Since the observed values of V_d are significantly less than unity, global mass conservation demands the presence of a by-pass stream. These by-pass pathlines were depicted schematically in Fig. 5.

Figure 14 is an example of the tests performed to check the influence of start-up and boundary conditions. To test the importance of initial conditions, runs with a sudden start of the inner cylinder are compared with runs monitored after a slow acceleration of the cylinder (Fig. 14 shows results for an acceleration equal to $1.75\,s^{-2}$). The axial displacement of the vortices clearly does not depend on outlet geometry on start-up rate, at least for the range of variables studied here.

Two kinds of experiments are performed using particles: visualization runs, with particles continuously fed into the VFR, and injection of particles using the chromatography syringe, following the same procedure as for the tracer injections. The same trend is observed in all the cases, although a tendency for sedimentation is more apparent for the Maxazyme particles, which have higher density. If the inner cylinder rotation increases, nevertheless, it is always possible to drag up the particles. Figure 15 exemplifies some empirical results.

As mentioned previously, this work does not intend to fit generalized empirical relations: that would demand testing different geometric parameters (η and Γ) in a systematic way. Our approach is rather to use a VFR conveniently dimensioned for applications in bio-processes and study its behavior in depth. Nevertheless, it is interesting to consolidate all the results we have reached in a non-dimensional space. Figure 16 displays these curves, showing the drift velocity V_d as a function of Re_{ax} and Re_θ.

The effect of these flow patterns on the reactor performance will be the result of a trade-off among different phenomena. Supposing that Re_{ax} is fixed, an increase in rotation will slow the movement of vortices, and increase the flux through the by-pass around them. At the same time, the vortex/by-pass mass transfer will also be enhanced, as well as the intra-vortex mixing. Reducing the rotation, V_d approaches unity, the 'stack of vortices' hypothesis will be more consistent, bringing the system closer to a plug flow, at least with respect to the vortices displacement. On the other hand, intra-vortex dispersion will be lower, and the reactor performance may depend on adequate inlet configurations. If solid particles are present, it will be necessary to sustain a minimum rotation rate, depending on the particle buoyancy. The net effect of all these factors on reactant conversion will be checked in specific experiments, reported in a forthcoming paper.

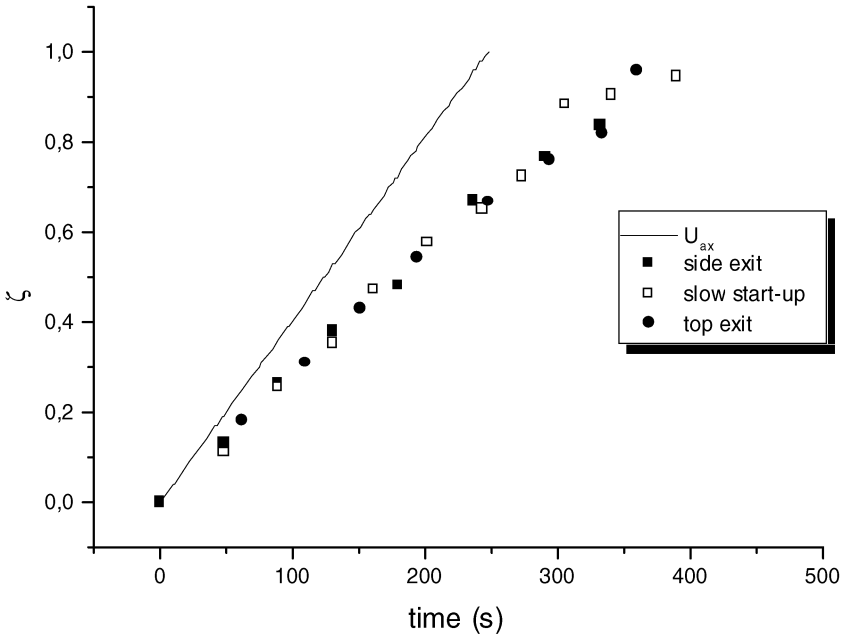

Fig. 14. Effect of start-up and boundary conditions on the vortex drift velocity. Axial flow rate: 1.67×10^{-7} m^3/s. Glycerol/water, 4.2 M, $\mu = 3.0 \times 10^{-3}$ kg/(m s). Tracer: blue dextran, $D_M = 3.0 \times 10^{-12}$ m^2/s. $T = 22°$C. Inner cylinder steady-state rotation rate: 4.71 s^{-1}.

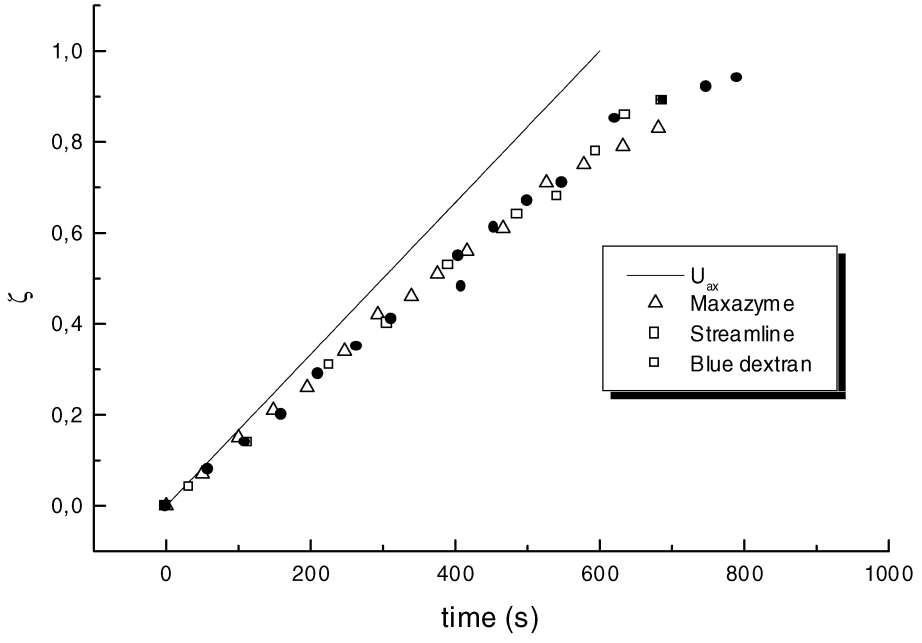

Fig. 15. Vortex drift velocity: tracer experiment compared with suspended particles. Axial flow rate: 7.94×10^{-8} m^3/s Glycerol/water, 4.2 M, $\mu = 3.0 \times 10^{-3}$ kg/(m s). Inner cylinder rotation = 3.04 s^{-1}. $T = 22°$C.

5. CONCLUSIONS

After performing a series of tracer injections and particle-visualization experiments in a Couette–Taylor–Poiseille apparatus with stationary outer cylinder, a flow pattern characterized by drift velocities less than unity in the low Re_{ax} region is identified. Increasing the rotation rates, it is possible to force the vortices to a full stop. Up to the best of our knowledge, this pattern has not been predicted until now by theory.

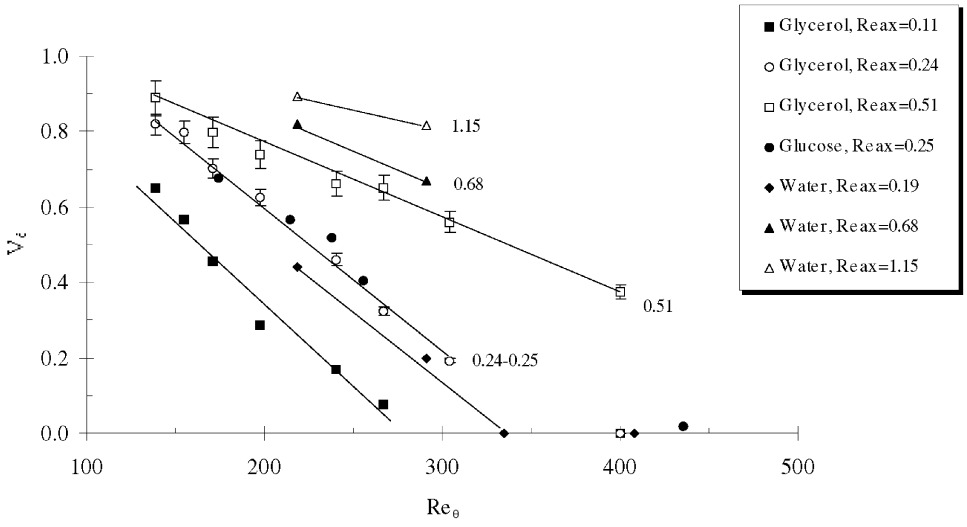

Fig. 16. Taylor–Couette–Poiseiulle flow: vortex drift velocities for different fluids, as a function of axial and rotational Reynolds numbers. Error bars illustrate the accuracy of the data for two typical experimental data sets.

The usual theoretical approach to determine the modes of the solution for the disturbances starts with a fully developed, laminar, Couette–Poiseuille basic flow, and than computes possible bifurcations. To be consistent with this approach, the drift velocity V_d has to be greater than unity in order to reach the absolutely unstable region (where the vortices would fill all the length of the apparatus). Our experiments point out a different reality, at least for the reactor configuration studied here.

These results, besides a purely theoretical interest, have important consequences in the modeling, design and optimization of VFRs. The combination of reactor geometry and flow rates studied here could be adequate for several distinct applications. It is important, therefore, to recognize (and to try to predict) the flow patterns that occur in this situation. This knowledge is essential to reliably forecast VFR performances and to have a base to decide on the convenience of its application in real-life processes.

Acknowledgements

'A System For Heparin Removal', Robert S. Langer, Steffen Ernst, Charles L. Cooney, supported by National Institute of Health, (GM 25810), MIT reference 63010. R. C. Giordano and R. L. C. Giordano thank for their grants (0078 and 0080/96) from CAPES (Brasilia, Brazil) and D. M. F. Prazeres thanks for a grant (7/B/96/PO) from NATO/JNICT (Portugal).

NOTATION

C	tracer concentration, M/l^3
C^0	mass of tracer injected/reactor volume, M/l^3
d	annular gap width ($=R_o - R_i$), l
D_{ax}	axial dispersion coefficient, l^2/T
D_M	tracer molecular diffusion coefficient, l^2/T
k	axial wave number ($=2\pi/\lambda$), l^{-1}
$K_{intervortex}$	inter-vortices mass transfer coefficient, l/T
L	axial length of the reactor, l
m	azimuthal wave number
r	radial coordinate, l
r'	dimensionless radial coordinate ($=r/d$)
R_i	inner (rotatory) cylinder radius, l
R_o	outer (stationary) cylinder radius, l
Re_θ	rotational Reynolds number ($=\omega R_i d/\nu$)
$Re_{\theta,c}$	critical rotational Reynolds number for the onset of Taylor vortices
Re_{ax}	axial Reynolds number ($=U_{ax}d/\nu$)
t	time, T
t'	dimensionless time ($=t\nu/d^2$)
U_{ax}	mean axial velocity, l/T
v_j	j-component of the velocity field, l/T
v'_j	disturbance of the j-component of the velocity with respect to the Couette–Poiseuille flow, l/T
V_d	vortex drift velocity (speed of the vortex center/U_{ax})
z	axial coordinate, l
z'	dimensionless axial coordinate ($=z/d$)

Greek letters

Γ	aspect ratio, ($=L/d$)
ζ	dimensionless distance from the point of injection (see Fig. 2) $\left[=\frac{(z-z_I)}{L}\right]$
η	radius ratio, ($=R_i/R_o$)
λ	axial wavelength (height of a pair of vortices), l
μ	viscosity, M/l T
ν	kinematic viscosity, l^2/T
σ	growth rate of the disturbance

τ ratio of the characteristic time for convection to that for intra-vortex diffusion, $(=LD_M/U_{ax}d^2)$, T
τ_m VFR mean residence time $(=L/U_{ax})$, T
ω disturbance oscillation frequency

REFERENCES

Andereck, C. D., Liu, S. S. and Swinney, H. L. (1986) Flow regimes in a circular Couette system with independently rotating cylinders. *J. Fluid Mech.* **164**, 155–183.

Ashwin, P., Mann, G. W. and King, G. P. (1995) Azimuthally propagating ring vortices in a model for nonaxisymmetric Taylor vortex flow. *Phys. Rev. Lett.* **75**, 4610–4613.

Barcilon, A., Brindley, J., Lessen, M. and Mobbs, F. R. (1979) Marginal instability in Taylor–Couette flows at a very high Taylor number. *J. Fluid Mech.* **94**, 453–463.

Brenan, K.E., Campbell, S.L. and Petzold, L.R. (1989) *Numerical Solution of Initial-Value Problems in Differential-Algebraic Equations*. Elsevier, New York.

Büchel, P., Lücke, M., Roth, D. and Schmitz, R. (1996) Pattern selection in the absolutely unstable regime as a nonlinear eigenvalue problem: Taylor vortices in axial flow. *Phys. Rev E* **53**, 4764–4777.

Campero, R. J. and Vigil, R. D. (1997) Axial dispersion during low Reynolds number Taylor–Couette flow: intra-vortex mixing effects. *Chem. Engng Sci.* **52**, 3303–3310.

Chandrasekhar, S. (1961) *Hydrodynamic and Hydromagnetic Stability*. Clarendon Press, Oxford.

Chossat, P. and Iooss, G. (1992) *The Couette–Taylor Problem*. Springer, Berlin.

Cohen, S. and Maron, D. M. (1991) Analysis of a rotating annular reactor in the vortex flow regime. *Chem. Engng Sci.* **46**, 123–134.

Coles, D. (1965) Transition in circular Couette flow. *J. Fluid Mech.* **21**, 385–425.

Davey, A. (1962) The growth of Taylor vortices in flow between rotating cylinders. *J. Fluid Mech.* **14**, 385–425.

Davey, A., Di Prima, R. C. and Stuart, J. T. (1968) On the instability of Taylor vortices. *J. Fluid Mech.* **31**, 17–52.

Desmet, G., Verelst, H. and Baron, G. V. (1996a) Local and global dispersion effects in Couette–Taylor flow — I. Description and modeling of the dispersion effects. *Chem. Engng Sci.* **51**, 1287–1298.

Desmet, G., Verelst, H. and Baron, G. V. (1996b) Local and global dispersion effects in Couette–Taylor Flow — II. Quantitative measurements and discussion of the reactor performance. *Chem. Engng Sci.* **51**, 1299–1309.

Desmet, G., Verelst, H. and Baron, G. V. (1997a) Transient and stationary axial dispersion in vortex array flows — I. Axial scan measurements and modeling of transient dispersion effects. *Chem. Engng Sci.* **52**, 2383–2401.

Desmet, G., Verelst, H. and Baron, G. V. (1997b) Transient and stationary axial dispersion in vortex array flows — II. Decoupling of inter- and intra-vortex transport phenomena. *Chem. Engng Sci.* **52**, 2403–2419.

Di Prima, R. C. and Swinney, H. L. (1985) Instabilities and transition in flow between concentric rotating cylinders. In *Hydrodynamic Instabilities and the Transition to Turbulence*, 2nd ed., eds H. L. Swinney and J. P. Gollub, pp. 139–180, Springer, Berlin.

Esser, A. and Grossman, S. (1996) Analytic expression for Taylor–Couette stability boundary. *Phys. Fluids* **8**, 1814–1818.

Gu, Z. H. and Fahidy, T. Z. (1985a) Visualization of flow patterns in axial flow between horizontal coaxial rotating cylinders. *Can. J. Chem. Engng* **63**, 14–21.

Gu, Z. H. and Fahidy, T. Z. (1985b) Characteristics of Taylor vortex structure in combined axial and rotating flow. *Can. J. Chem. Engng* **63**, 710–715.

Gu, Z. H. and Fahidy, T. Z. (1986) The effect of geometric parameters on the structure of combined axial and Taylor-vortex flow. *Can. J. Chem. Engng* **64**, 185–189.

Haim, D. and Pismen, L. M. (1994) Performance of a photochemical reactor in the regime of Taylor–Görtler vortical flow. *Chem. Engng Sci.* **49**, 1119–1129.

Kataoka, K. (1975) Heat-transfer in a Taylor vortex flow. *J. Chem. Engng Japan* **8**, 271–276.

Kataoka, K., Doi, H., Komai, T. and Futagawa, M. (1975) Ideal plug flow properties of Taylor vortex flow. *J. Chem. Engng Japan* **8**, 472–476.

Kataoka, K., Ohmura, N., Kouzu, M., Simamura, Y. and Okubo, M. (1995) Emulsion polymerization of styrene in a continuous Taylor vortex flow reactor. *Chem. Engng Sci.* **50**, 1409–1416.

Kataoka, K. and Takigawa, T. (1981) Intermixing over cell boundary between Taylor vortices. *A.I.Ch.E. J.* **27**, 504–508.

Koschmieder, E. L. (1979) Turbulent Taylor vortex flow. *J. Fluid Mech.* **93**, 515–527.

Koschmieder, E. L. (1993) *Bénard Cells and Taylor Vortices*. Cambridge University Press, New York.

Lathrop, D. P., Fineberg, J. and Swinney, H. L. (1992) Turbulent flow between concentric rotating cylinders at large Reynolds number. *Phys. Rev. Lett.* **68**, 1515–1518.

Legrand, J., Coeuret, F. and Billon, M. (1983) Struture Dynamique et Transfert de Matière Liquide-Paroi dans le Cas de l'Écoulement Laminaire Tourbillonnaire de Couette–Poiseuille. *Int. J. Heat Mass Transfer* **2**, 1075–1085.

Legrand, J. and Coeuret, F. (1986) Circumferential mixing in one-phase and two-phase Taylor vortex flows. *Chem. Engng Sci.* **41**, 47–53.

Legrand, J. and Coeuret, F. (1987) Transfert de Matière Liquide-Paroi et Hydrodynamique de l'Écoulement de Couette-Taylor-Poiseuille Biphasique. *Can. J. Chem. Engng* **65**, 237–243.

Lueptow, R. M., Docter, A. and Min, K. (1992) Stability of axial flow in an annulus with a rotating inner cylinder. *Phys. Fluids A* **4**, 2446–2455.

Lueptow, R. M. and Hajiloo, A. (1995) Flow in a rotating membrane plasma separator. *A.S.A.I.O. J.* **41**, 182–188.

Marcus, P. S. (1984a) Simulation of Taylor–Couette flow. Part 1. Numerical methods and comparison with experiment. *J. Fluid Mech.* **146**, 45–64.

Marcus, P. S. (1984b) Simulation of Taylor–Couette flow. Part 2. Numerical results for wavy-vortex flow with one traveling wave. *J. Fluid Mech.* **146**, 65–113.

Moore, C. M. V. and Cooney, C. L. (1995) Axial dispersion in Taylor-Couette flow. *A.I.Ch.E. J.* **41**, 723–727.

Ng, B. S. and Turner, E. R. (1982) On the linear stability of spiral flow between rotating cylinders. *Proc. Roy. Soc. London A* **382**, 83–102.

Ohmura, N., Kataoka, K., Shibata, Y. and Makino, T. (1997) Effective mass diffusion over cell boundaries in a Taylor-Couette flow system. *Chem. Engng Sci.* **52**, 1757–1765.

Pudjiono, P. I., Tavare, N. S., Garside, J. and Nigam, K. D. P. (1992) Residence time distribution from a continuous couette flow device. *Chem. Engng J.* **48**, 101–110.

Pudjiono, P. I. and Tavare, N. S. (1993) Residence time distribution analysis from a continuous Couette flow device around critical Taylor number. *Can. J. Chem. Engng* **71**, 312–318.

Rayleigh, Lord (1916) On the dynamics of revolving fluids. *Proc. Roy. Soc. London A* **93**, 148–154.

Recktenwald, A., Lücke, M. and Müller, H. W. (1993) Taylor vortex formation in axial through-flow: linear and weakly nonlinear analysis. *Phys. Rev. E* **48**, 4444–4454.

Sczechowski, J. G, Koval, C. A. and Noble R. D. (1995) A Taylor vortex reactor for heterogeneous photocatalysis. *Chem. Engng Sci.* **50**, 3163–3173.

Snyder, H. A. (1962) Experiments on the stability of spiral flow at low axial Reynolds numbers. *Proc. Roy. Soc. London A* **265**, 198–214.

Stuart, J. T. (1958) On the non-linear mechanics of hydrodynamic stability. *J. Fluid Mech.* **4**, 1–21.

Stuart, J. T. (1986) Taylor-vortex flow: a dynamical system. *S.I.A.M. Rev.* **28**, 315–342.

Tagg, R. (1992) A guide to literature related to the Taylor–Couette problem, In *Ordered and Turbulent Patterns in Taylor–Couette Flow*, eds. C. D. Andereck and F. Hayot, p. 303. Plenum Press, New York.

Takeuchi, D. I. and Jankowski, D. F. (1981) A numerical and experimental investigation of the stability of spiral poiseuille flow. *J. Fluid Mech.* **102**, 101–126.

Tam, W. Y. and Swinney, H. L. (1987) Mass transport in turbulent Couette–Taylor flow. *Phys. Rev. A* **36**, 1374–1381.

Taylor, G. I. (1923) Stability of a viscous liquid contained between two rotating cylinders. *Phil. Trans. R. Soc. A* **223**, 289–343.

Tsameret, A. and Steinberg, V. (1994a) Absolute and convective instabilities and noise-sustained structures in the Couette–Taylor system with an axial flow. *Phys. Rev. E* **49**, 1291–1308.

Tsameret, A. and Steinberg, V. (1994b) Competing states in a Couette–Taylor system with an axial flow. *Phys. Rev. E* **49**, 4077–4086.

Villadsen, J. V. and Michelsen, M. L. (1978) *Solution of differential Equation Models by Polynomial Approximation.* Prentice-Hall, Englewood Cliffs, NJ.

Wei, T., Kline, E. M., Lee, S. H.-K. and Woodruff, S. (1992) Görtler vortex formation at the inner cylinder in Taylor–Couette flow. *J. Fluid Mech.* **245**, 47–68.